applied sciences

MDPI

Article

Modeling and Measurement of Tool Wear During Angular Positioning of a Round Cutting Insert of a Toroidal Milling Tool for Multi-Axis Milling

Michał Gdula [1,*], Lucia Knapčíková [2], Jozef Husár [2] and Radoslav Vandžura [3]

[1] Department of Manufacturing Techniques and Automation, Faculty of Mechanical Engineering and Aeronautics, Rzeszow University of Technology, al. Powstańców Warszawy 12, 35-959 Rzeszów, Poland
[2] Department of Industrial Engineering and Informatics, Faculty of Manufacturing Technologies, Technical University of Košice, Bayerova 1, 080 01 Prešov, Slovakia; lucia.knapcikova@tuke.sk (L.K.); jozef.husar@tuke.sk (J.H.)
[3] Department of Automobile and Manufacturing Technologies, Faculty of Manufacturing Technologies, Technical University of Košice, Šturova 31, 080 01 Prešov, Slovakia; radoslav.vandzura@tuke.sk
* Correspondence: gdulam@prz.edu.pl; Tel.: +48-17-865-1372

Abstract: The aim of this study was to develop a concept for an angular positioning method for a round cutting insert in a torus cutter body dedicated to the multi-axis milling process under high-speed machining cutting conditions. The method concept is based on a developed wear model using a non-linear estimation method adopting a quasi-linear function. In addition, a tool life model was developed, taking into account the cutting blade work angle parameter, the laser marking method for the round cutting insert, and a wear measurement methodology. The developed tool wear model provides an accuracy of 90% in predicting the flank wear of the cutting blade. The developed procedure for angular positioning of the round cutting insert enables the entire cutting edge to be fully utilized, extending the total tool life. In addition, the measured largest defect values between the worn cutting edge and the nominal outline of the round cutting insert indicate the location of notching-type wear.

Keywords: multi-axis machining; torus milling cutter; angular positioning; round cutting insert; tool wear modeling; optical and digital measurements

Citation: Gdula, M.; Knapčíková, L.; Husár, J.; Vandžura, R. Modeling and Measurement of Tool Wear During Angular Positioning of a Round Cutting Insert of a Toroidal Milling Tool for Multi-Axis Milling. *Appl. Sci.* **2024**, *14*, 10405. https://doi.org/10.3390/app142210405

Academic Editor: Mark J. Jackson

Received: 24 September 2024
Revised: 31 October 2024
Accepted: 6 November 2024
Published: 12 November 2024

1. Introduction

Continuous technological advances in the aerospace and energy industries, as well as molds and dies, are resulting in the increasing use of difficult-to-cut materials for responsible machine parts [1–5]. This necessitates the need for methods and strategies to extend the life of cutting tools. Difficult-to-cut materials, i.e., Ti alloys, Ni-based superalloys, and hardened steels, are generally characterized by low thermal conductivity and high hardening, which makes machining at high cutting speeds significantly more difficult. These are the main reasons for the rapid wear of tools, which has a negative impact on both the cutting process and the technological surface layer [6–9]. Therefore, tool wear is one of the main challenges in the precision machining of difficult-to-cut materials, especially nowadays in multi-axis machining [10,11].

In industrial practice, the torus milling cutter is increasingly being used to machine the surfaces of geometrically complex parts. This cutter, both in its monolithic form and essentially in the form of indexable round cutting inserts, is used especially in the finishing stage, mainly because of its unique geometry [12]. The vast majority of the work concerns the torus milling cutter in terms of the mechanics of the cutting process [12–15]. From the analysis of the issue to date, it appears that there is a lack of work that addresses the angular positioning of the round cutting inserts in the torus cutter body. This positioning

would aim to utilize all possible active cutting edge segments on the circle of the cutting insert in a given fixed tool axis orientation.

Positioning is defined as the exact location of a given object relative to an assumed reference point or line, which is usually the origin of a given Cartesian Coordinate System. Positioning, or more precisely, precise positioning, is also widely used in many areas of mechanical engineering, especially in the era of the Industry 4.0 industrial revolution [16]. In this case, the most tangible examples of precision positioning tasks are as follows: locating the probe of a measuring instrument relative to the measurement target, determining the position of the cutter relative to the workpiece, montaging a screw in the target hole using a robot arm, etc. All examples of engineering tasks related to precise positioning described above are supported by advanced systems and technologies, including measurement systems [16–26].

The measurement basis for precise positioning are the latest sensor technologies for single-axis, linear, or rotational measurements. The vast majority of practical applications require positioning in a plane or in a 3D space, and one of the most frequently used ones is angular positioning. These are realized by multi-axis coordinate measurement methods, such as triangulation and multilateration, as well as measurements in Cartesian and polar systems. The work in [27] presents the results of measuring the deviation of the shaft diameter after the turning process using the LTS laser triangulation sensor. A program was developed and verified whose task is to communicate between the PLC controller in the measurement system and the software for recording data obtained from the LTS laser triangulation sensor. In this case, inspection of the manufactured product is one of the most important operations in the technological production process [28]. Based on the test results, the authors concluded that this type of sensor is suitable for measuring the deviation parameter of the diameter of the machined surface. Another important issue is to reduce the positioning error of the rotary table of a multi-axis machine tool. The angular positioning error in this case causes poor quality milling of the workpiece surface. Therefore, in [29], the authors developed a system to improve this issue, using the Laser R-Test to calibrate angular positioning and compensate for positioning errors of the numerically controlled axes of the machine tool. Uncertainty analysis and calibration were implemented to predict the system. As evaluated by the authors of this work, the proposed measurement method can also solve the problems of coaxiality between the measuring devices and the rotary table. The system developed in this work achieves an angular error of 0.00121° for real workpieces, which is smaller than the error achieved by the commercial system, which is approximately 0.0022°. In turn, in [30], the angular positioning error of the rotary axis caused by the tilt movement error and the spindle radial movement error was analyzed and experimentally verified. In addition, the offset value introduced to the encoder was analyzed and experimentally verified. Angular positioning is also an important parameter that determines the proper operation of force systems. Hence, in [31], a non-contact optical sensing method was developed to simultaneously detect the linear and angular position of the rotor of a prototype 2DOF-SRM reluctance motor. In [32], the authors proposed a method for calibrating the angular positioning deviation of a precision rotary table of a coordinate measuring machine based on a measurement system with a laser marker. The Levenberg–Marquardt algorithm and the singular value distribution transformation were used to calculate the coordinates of the laser marker station. The fixed-interval angular deviation was calibrated using a geometric relationship model between the coordinates of the laser marker station and the rotation angle of the turntable. The work in [33] presents an angular position measurement system based on a sensor consisting of a single transmitter and two receiving coils. The mutual inductance between the transmitter coils was spatially modulated using conductive lenses. The measurement results form the basis for estimating the absolute angle. The advantage of this solution is resistance to many harmful factors, such as moisture, poor lighting, or oil contamination. Therefore, this system could be successfully used for angular positioning, e.g., indexable cutter blades. Angular positioning is also important from a military point of view. In [34], a system

was developed based on an algorithm to calculate the angular position of the rocket in real time when it is ready to launch from the rocket launcher. For this purpose, video streams recorded from three different cameras were used. Finally, the algorithm was implemented on a programmable SoPC chip using FPGA programmable array gates. In addition to systems based on sensors or optics, flexible mechanical systems are also used for precise angular positioning [35]. These are usually flexible micro-angular position measurement systems.

However, in order to measure along with determining the positioning of the circular cutting edge insert, it is necessary to know after what time this insert needs to be turned in the cutter body due to wear. For this, there is a need to develop tool wear and life models. In terms of multi-axis milling, Luo et al. [11] proposed such a model, but it is a linear model. The linear model does not predict the variable nature of wear progression during the operational wear progression phase. Hence, in this thesis, a non-linear estimation is proposed that predicts this variable nature.

The purpose of this study is to develop the basis for an angular positioning method for the circular cutting insert of a torus cutter that takes into account its wear and life. To achieve this, the parameters for the orientation of the tool axis with respect to the normal vector of the machined surface and the technique for avoiding undercutting the machined surface in multi-axis milling were first defined. A relationship was then determined for the working angle of the cutting blade, which is also a parameter controlling the orientation of the tool axis, and in its range, the wear progress of the active cutting edge segment is observed. A study of the machinability of the selected material was carried out, and a life and wear model for the torus milling cutter was developed from the resulting database. Integral to the above steps and the proposed method are measurements of tool wear and angle for angular positioning of the round cutting insert. The paper concludes with conclusions and the identification of directions for further research.

2. Fundamentals of the APofRCI Method, Taking into Account Torus Milling Cutter Cutting Blade Wear

In multi-axis face milling, the milling cutter can have any orientation in the Cartesian space when machining a sculptured surface, assuming, of course, that there is no collision—in the sense of undercutting. Consequently, different tool orientations can also be defined for a given toolpath. The geometrical characteristics of the milling cutter used for machining, the geometrical characteristics of the machined surface, and the resulting contact conditions (CWE: cutter-workpiece engagement) between the tool and the machined surface must also be taken into account.

2.1. Definition of the Torus Milling Cutter Axis Orientation

In the present work, in order to obtain the orientation of the tool axis for the kinematic variant of TPL (tool pulling) multi-axis cutting, the inclination angle was used as the process adjustment variable. In the present work, in order to obtain the tool axis orientation for the kinematic variant of TPL (tool pulling) multi-axis cutting, the inclination angle was used as the process adjustment variable. It is the same as the advance angle in this variant. The lead angle β, along with the tilt angle α, is an essential adjustable variable in CAM systems at the pre-processing stage. On the other hand, in the NC code, based on the conversion relationship between angles β and α, the inclination angle setpoint adjustable variable δ obtained in the post-processing stage of the CAM system is derived and, in this version, interpreted by the CNC control of the machine tool. Figure 1 illustrates the set variables of the tool axis, and the conversion relationship is described by Equation (1). Equation (2) defines the condition when the inclination angle is the same as the lead angle.

$$\delta = \cos^{-1}[\cos(\alpha)\cdot\cos(\beta)], \tag{1}$$

$$\beta = \delta, \quad \text{when}: \ \alpha = 0^{\circ}, \tag{2}$$

where β is the lead angle; α is the tilt angle; and δ is the inclination angle.

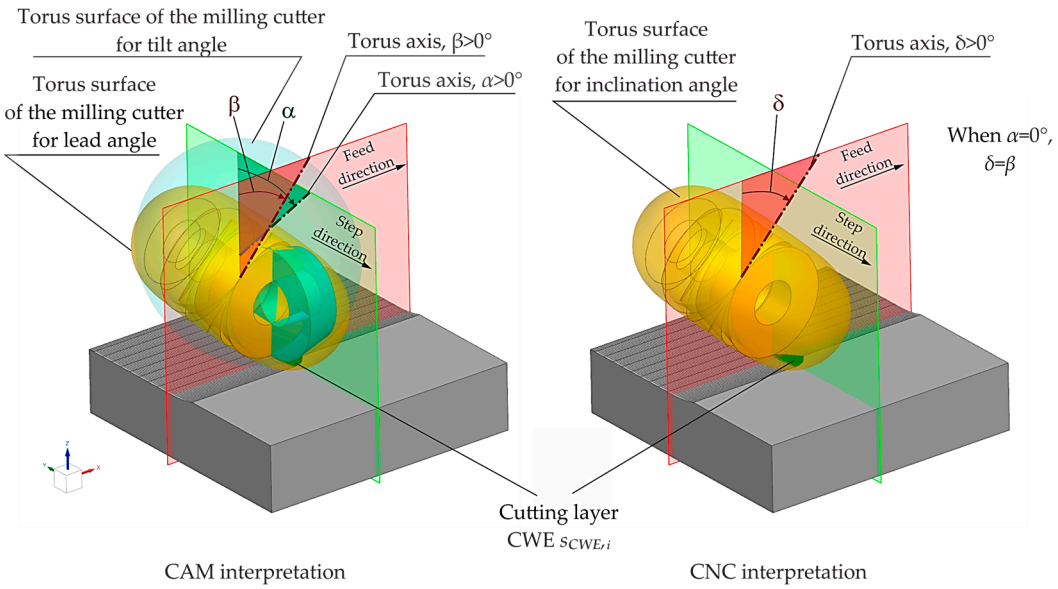

Figure 1. Tool axis orientation and its interpretation at pre-processor and post-processor stages.

2.2. Characteristics of the Torus Milling Cutter

In industrial practice, torus cutters are increasingly used in the multi-axis face milling process of TPL. These cutters enable larger cutting widths to be achieved, allowing efficiency to increase and machining time to be reduced. The design of torus cutters also allows higher cutting speeds and feed rates to be used. These are usually folding cutters with indexable Round Cutting Inserts (RCIs) for nominal diameters of these cutters from 12 mm.

The design advantage of this type of cutter is that the indexable round cutting insert can be rotated around the axis of its mounting hole to use a new, unused cutting edge segment for machining. This allows the tool life to be significantly extended. Currently, this rotation is carried out without any control of the angular position of the round cutting insert, leading to an unreasonable use of the real segments of the cutting edge around its circumference. The tool life decreases. The possible cases are schematically illustrated in Figure 2.

The first illustrated case (Figure 2a) shows the overlap of part of a new cutting edge segment with a worn segment. This erroneous angular position can result in significant deterioration of the technological surface layer and progressive catastrophic tool wear. The second case (Figure 2b) illustrates the occurrence of an excessive gap between adjacent segments after uncontrolled rotation of the RCI. In turn, this erroneous angular position reduces the cutting capacity of the tool due to incomplete use of the entire cutting edge. In contrast, the third case (Figure 2c) illustrates a worn and new segment, directly adjacent to each other. This will only happen if the rotation of the round cutting insert around the axis of the mounting hole is controlled.

The main objective of this article is to develop an angular positioning method for the round cutting insert of the torus milling cutter that allows the full cutting potential of the entire edge of the insert to be exploited by adhering segments with uniform angular dividing.

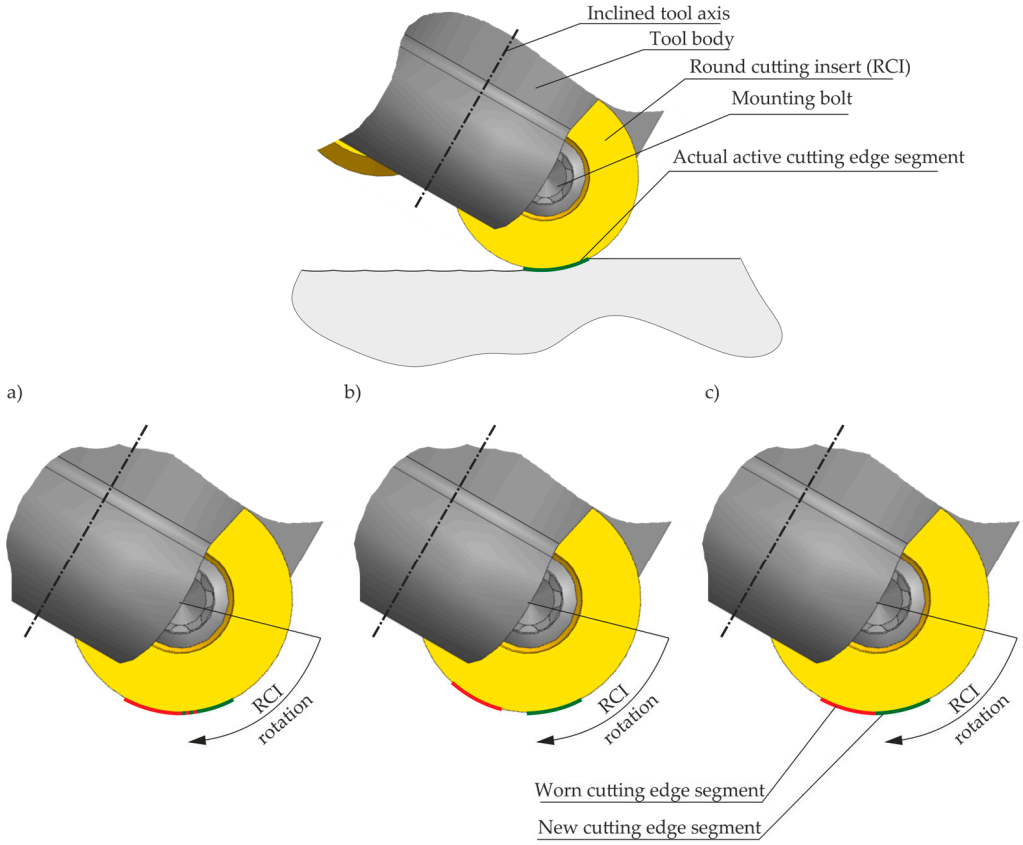

Figure 2. Possible cases of the round cutting insert rotation: (**a**) overlapping of a new segment with a worn segment—wrong; (**b**) too large a gap between segments—wrong; (**c**) segments adjacent to each other—correct.

2.3. Method to Avoid Undercutting the Machined Surface

In order to develop an angular positioning method for round cutting inserts of the torus milling cutter, dedicated to the multi-axis milling process, it is first necessary to determine the minimum required inclination angle δ. The minimum inclination angle required is to ensure that the torus milling cutter axis is positioned in such a way that no undercutting of the workpiece surface occurs. Three surface types were selected in terms of shape: biconcave, saddle concave-convex, and saddle convex-concave. The selected sculptured surfaces are described by a radius of curvature radius ρ parameter (the inverse of the curve curvature) in the feed direction ρ_1 and in the direction perpendicular to the feed ρ_2, respectively. A negative sign was assumed for the radius of convex curvature and a positive sign for the radius of concave curvature, as illustrated in Figure 3.

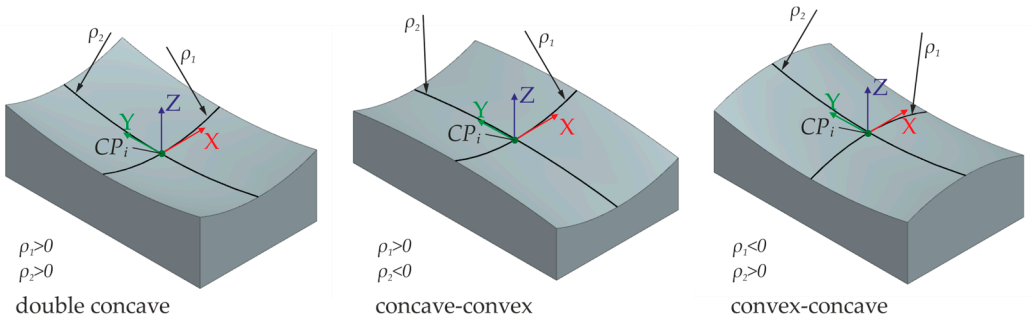

Figure 3. Types of sculptured surfaces.

A sphere of radius R was used to determine the position of the tool in a way that excludes the possibility of the torus undercutting the machined surface. This method was first defined by Marciniak [36]. The common part of the sphere and the torus is the contact diameter, and the local position of the tool determines the contact between the torus and the machined surface at the CP_i contact point, as shown in Figure 4. The inclination angle δ of the tool axis is defined relatively to the nornal vector $n(CP_i)$ of the machined surface at the contact point CP_i. In generalizing the problem, the machined surface was assumed to be a strictly tangential plane. This plane, in turn, is a simplified model of any type of sculptured surface at the contact point between the torus and the machined surface.

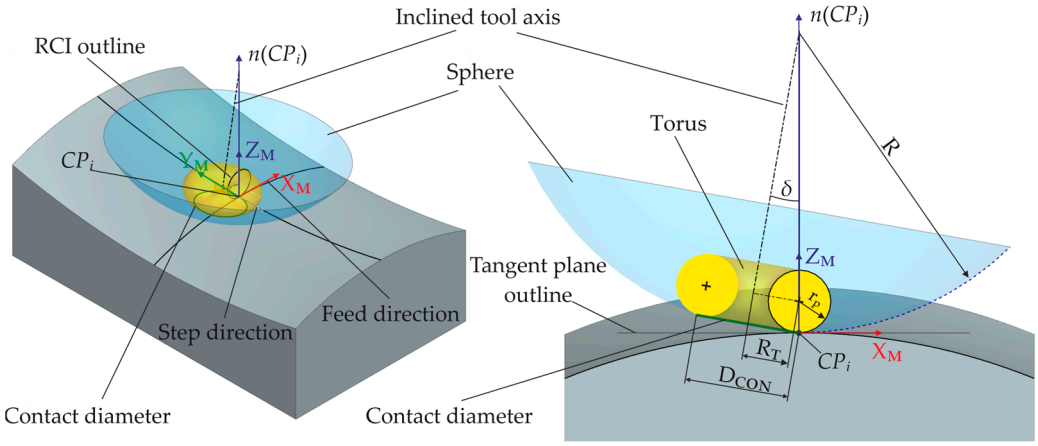

Figure 4. Method of detecting undercutting of the machined surface by the torus of the cutter.

The radius of sphere R can be determined using Equation (3).

$$R = \frac{R_T}{\sin(\delta)} + r_p, \tag{3}$$

where R_T is the radius of the torus milling cutter (the tool rotation axis of distance of the torus from the center of the RCI outline defining it); δ is the inclination angle; r_p is the radius of the round cutting insert (the circle defining the torus).

The undercutting of the machined surface by the torus does not occur when Equation (4) is fulfilled.

$$R \leq \rho_1, \rho_2, \tag{4}$$

where ρ_1 is the smallest radius of concave curvature in the feed direction; ρ_1 is the smallest radius of concave curvature in the step direction.

The above condition must be met for concave contours (for which the curvature has a positive sign). For convex contours, for $\delta \geq 0°$, undercutting does not occur.

Hence, Equation (5) applies to calculate the minimum inclination angle δ_{min}, depending on the nominal diameter.

$$\delta_{min} = \sin^{-1}\left(\frac{R_T}{\rho - r_p}\right), \tag{5}$$

It is assumed that there are no large changes in curvature in the immediate vicinity of the contact point CP_i in the CWE that could lead to undercutting. Therefore, once calculated, the δ_{min} parameter is used as a constant value along the entire contour of the machined surface, and the tool axis is oriented in the Cartesian space relative to the normal vector $n(CP_i)$ of the machined contour.

2.4. Active Cutting Edge Segment and Active Cutting Belt

Basically, the inclination angle δ is spread and determined in a plane perpendicular to the cutting speed vector v_c and passing through the contact point CP_i in the CWE, which is the common point of the outline of the machined surface and the cutting edge of the tool blade. The geometry of the cut layer is considered in the same plane. The geometrical parameters of the cut layer have a significant influence on the physical and technological effects of the cutting process, especially multi-axis milling.

During multi-axis TPL-type milling using the torus milling cutter, the geometry of the cut layer has a characteristic shape, where, due to the kinematic-geometric system, the thickness of the cut layer h varies along the cutting edge, as shown in Figure 5a. The geometry of the cut layer is influenced by the radius of the round cutting insert r_p, the feed per tooth f_z, and the depth of cut a_p.

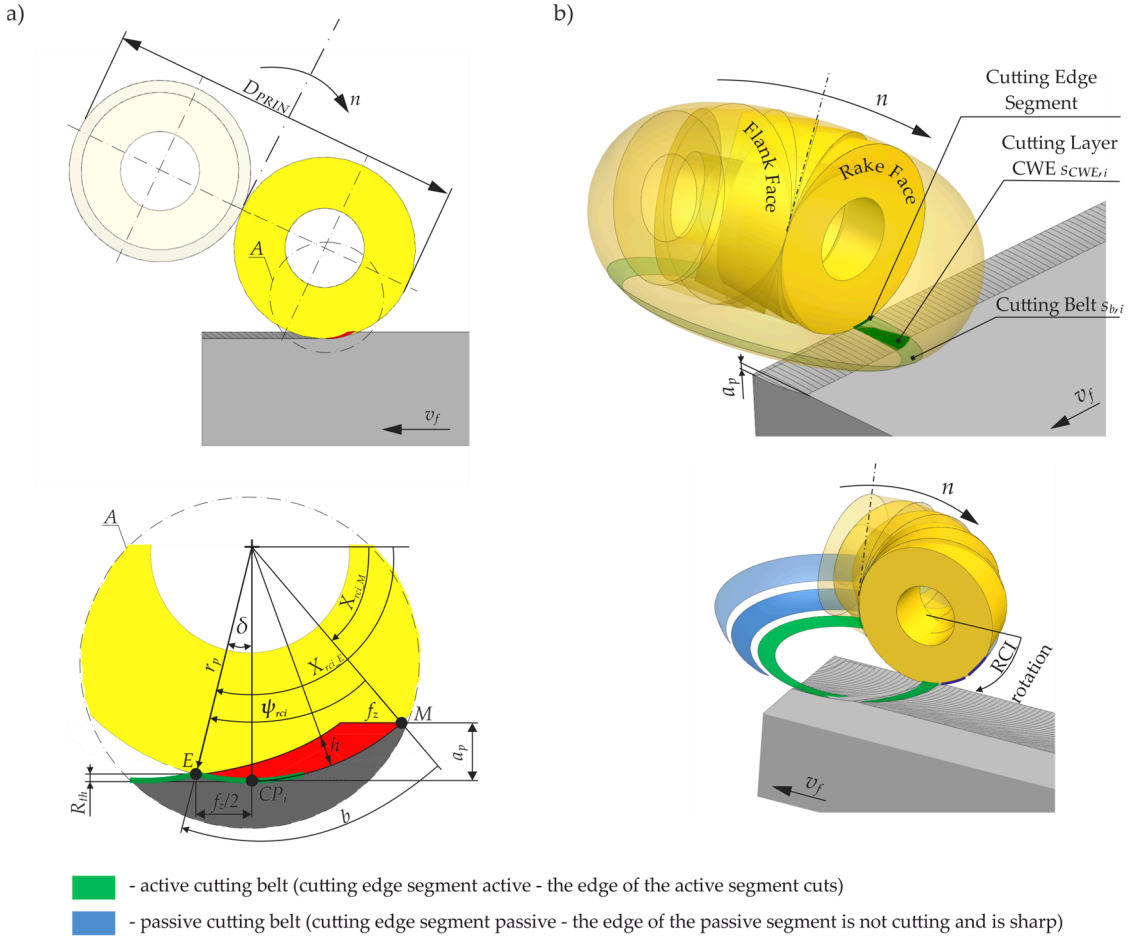

Figure 5. Multi-axis milling using the torus milling cutter: (**a**) cut layer geometry; (**b**) active cutting edge segment and active cutting belt.

By considering the contact conditions in the CWE at the CP_i contact point, the angles X_{rci_M}, X_{rci_E}, and ψ_{rci} were determined to determine the maximum cross-sectional limits of the cut layer.

Angle X_{rci_M}—the angle defining the origin of the cross-section of the cut layer, as described in Equation (6).

$$X_{rci\_M} = \sin^{-1}\left(1 - \frac{a_p}{r_p}\right), \quad (6)$$

Angle X_{rci_E}—the angle defining the end of the cross-section of the cut layer, as described in Equation (7).

$$X_{rci\_E} = \frac{\pi}{2} + \sin^{-1}\left(\frac{f_z}{2r_p}\right), \tag{7}$$

Angle ψ_{rci}—working angle of the torus milling cutter, considered in the base plane of the round cutting insert at the CP_i contact point, as described in Equation (8).

$$\psi_{rci} = \left[\frac{\pi}{2} + \sin^{-1}\left(\frac{f_z}{2r_p}\right) - \sin^{-1}\left(1 - \frac{a_p}{r_p}\right)\right], \tag{8}$$

Equation (8) is an important and rarely analyzed relationship in the literature. It acquires particular importance, especially under the conditions of finish machining, which takes place at very small values of depth of cut a_p and feed per tooth f_z. Under these cutting conditions, the number of involved cutting blades (active blades) of the tool in the cutting process is $z_c \leq 1$ [37]. Knowing the value of the angle ψ_{rci} and having the given radius r_p of the round cutting insert, the length of the active segment of the cutting edge b can be calculated using Equation (9).

$$b = \psi_{rci} r_p, \tag{9}$$

Thus, the active cutting belt can be determined (see Figure 5b) for a given inclination angle δ in the CWE. During the movement of the tool, the tool is in contact with the workpiece on a temporary patch of the machined surface, which is called Cutter-Workpiece Engagement (CWE), and the material removed is the cut layer in the form of a chip. The CWE is located on the torus action surface of the tool within the adopted depth of cut a_p. As the tool rotates about its axis, the CWE $s_{CWE,i}$ at the contact point forms a belt $s_{b,i}$, which was named the cutting belt, and is located on the action surface of the torus milling cutter. At any moment of cutting, the segment on the cutting edge that is inside the CWE is called the active segment of the cutting edge, i.e., the edge of the active segment is cutting at that moment. In addition, segments that are outside the CWE have been identified that are passive cutting edge segments, where the edge of the passive segment does not cut and is sharp.

The angle parameter ψ_{rci} in this work is used as the main parameter for the angular positioning of the round cutting insert in the torus milling cutter body, which is a new and original solution and the basis of the angular positioning method of the round cutting insert. In order to know after what time an active cutting edge segment is unusable (for an assumed *VB* criterion) and what the nature of the wear is at each time interval, both a tool wear model and a tool life model must be developed.

2.5. The Torus Milling Cutter Wear and Life Model

The wear rate of a torus milling cutter reflects the wear rate at any point on the active cutting edge, which is a part in common with the torus action surface and depends on the inclination angle. Importantly, it changes during machining. Figure 6 shows a typical tool wear curve as a function of the cutting time at a certain constant cutting speed. It presents a classic three-phase course. During phase I—the initial phase—tool wear increases dramatically and reaches its baseline value in a short period of time. In phase II, wear and tear of a quasi-linear and difficult-to-predict nature can be observed. Phase III is characterized by accelerated wear until a critical value associated with blade failure is reached.

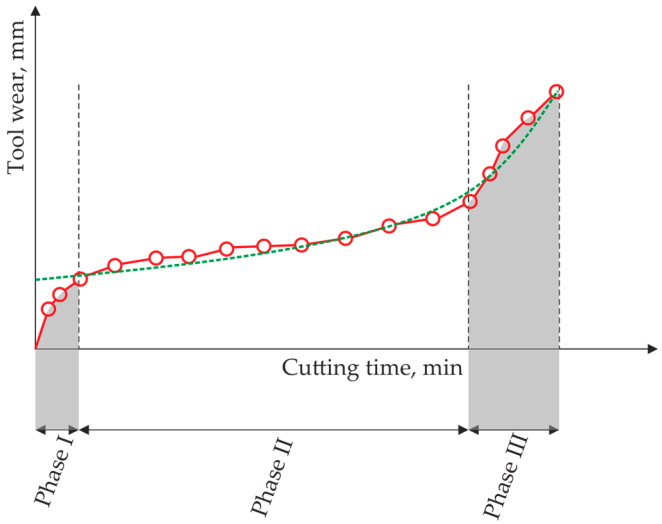

Figure 6. Typical tool wear rate at a constant cutting speed.

Furthermore, for wear modeling (dotted green line), i.e., using regression analysis [38–40], phase I can be neglected, and the tool wear at any cutting point on the torus action surface can be considered as a variable over time (such as in accelerated motion) and described by the model of an exponential function, which is expressed by Equation (10).

$$VB_{Bmax} = b_0 \cdot b_1^{t_c}, \tag{10}$$

where VB_{Bmax}—maximum abrasion width, an important indicator in multi-axis finish milling; b_0 and b_1—coefficients determined for a given material pair, i.e., round cutting insert—workpiece, and machining conditions; t_c—cutting time. The b_0 and b_1 coefficients are constituted on the basis of machinability tests and non-linear estimation analysis.

The tool is used for machining with the declared fixed machining parameters until the tool wear reaches the adopted critical value VB_{Blim} at time T_t. The value of time T_t, i.e., the tool life, is expressed by Equation (11):

$$T_t = C_t \cdot v_c^p \cdot f^q, \tag{11}$$

where T_t—the tool life; v_c—the cutting speed at the selecting cutting point; and f is the feed rate. C_t, p, and q are certain constants for a given material pair, i.e., the material of the round cutting insert material of the workpiece. These constants are constituted on the basis of calibrated machinability tests. On this basis, the tool life is determined from which the C_t, p, and q factors are calculated.

When milling with a torus milling cutter, with the spindle speed set to an arbitrary and constant value, the cutting speed varies along the cutting edge from the cutter tip point (TCP) towards the tool attachment point in the spindle. The cutting speed $v_{c,g}$ at a point with height g from the apex of the TCP torus milling cutter is expressed by Equation (12):

$$v_{c,g} = \frac{2\pi n\left(R_T + \sqrt{2r_p g - g^2}\right)}{1000}, \tag{12}$$

where n is the spindle speed; R_T is the radius from the rotational axis of the tool to the center point of the round cutting insert; and r_p is the radius of the round cutting insert. As shown in Figure 7, the cutting speed varies significantly given the parameter g along the torus milling cutter axis. The cutting speed values $v_{c,g}$ in this case were simulated for a cutting angle in the range $0^\circ \leq \psi_{rci} \leq 23.4411^\circ$ in the tool base plane coinciding with the tool's feed speed plane v_f.

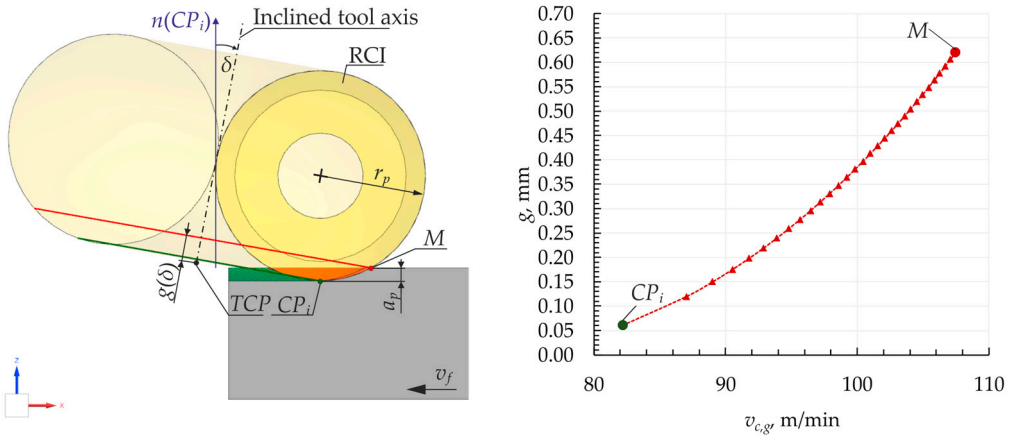

Figure 7. Cutting speed variation along the tool axis for torus milling cutter (tool diameter: 16 mm; round cutting insert radius: 4 mm; spindle speed: 2786 rpm; inclination angle: 10°).

Note that, assuming that both feed rate and the spindle speed are constant, the cutting speed $v_{c,g}$ depends only on the latitude g of the adopted cutting point, e.g., the contact point CP_i that falls within the length of the active cutting edge segment b. The latitude g is described in Equation (13).

$$g = r_p\left[1 - \cos\left(\frac{\pi}{2} - \sin^{-1}\left(1 - \frac{a_p}{r_p}\right)\right) + \delta\right], \tag{13}$$

where r_p is the radius of the round cutting insert; a_p is the depth of cut; and δ is the inclination angle.

For further considerations, the symbol $T_{c,g}$ is adopted to denote the tool wear rate of any point in the length of the active cutting edge segment b (i.e., in the active cutting strip $s_{b,i}$) at latitude g, as expressed by Equation (14) [11].

$$T_{c,g} = C_t\left(\frac{2\pi n\left(R_T + \sqrt{2r_p g - g^2}\right)}{1000}\right)^p f^q, \tag{14}$$

3. Machining and Measurement Conditions

3.1. Materials, Tools, and Machining Station

The Ni-based superalloy Inconel 718 was selected for machining tests. The TPL machining process was carried out using steel torus milling cutter body R300-016A20L-08L, dedicated to round cutting inserts R300-0828E-PL. The torus milling cutter as a tool assembly has a neutral geometry. The replaceable round cutting inserts are made of fine-grain carbide and coated with TiAlN anti-wear PVD technology. Round cutting inserts with a diameter of 8 mm were fitted into a tool body with a diameter of 16 mm at an overhang of 65 mm.

The machining station with experimental set-up is shown in Figure 8. A 5-axis CNC vertical machining center, model DMU 100 MonoBLOCK, was used to carry out machinability tests in the multi-axis TPL milling process. The tool life was determined by the wear VB_{Bmax} located on the lateral surface of the cutting edge until the adopted maximum value of the wear criterion VB_{Blim} was reached. The machining process was interrupted at specific intervals to collect data for modeling and wear calibration. Measurements were carried out using a DinoLite 7000 CE workshop microscope. The above-mentioned experimental workstation is at the equipment of the Department of Manufacturing Technics and Automation, seated in Rzeszów.

Figure 8. Experimental test bench (1. Machining tool, 2. Torus milling cutter, 3. Workpiece, 4. Dino-Lite 7000 CE series digital workshop microscope).

3.2. Tool Wear Modeling and Calibration

The research on tool wear and tool life, to develop a model and calibrate tool wear, involved a series of passes in a multi-axis milling process with a torus milling cutter, whose axis was deflected with respect to the normal vector of the machined surface in the feed direction by the inclination angle parameter δ (see Figure 1).

The experimental tests were carried out in two main stages. Flood cooling was used in all cutting tests. The cutting conditions were chosen on the basis of our own preliminary research and works [10,11,13,40]. The ambient temperature was 21°.

In the first stage, by carrying out machinability tests, data were obtained to develop a wear model using a non-linear estimation method. Cutting tests were carried out under HSM (High-Speed Machining). A constant cutting speed of v_c = 140 m/min was determined at the principal diameter of the torus D_{PRIN} (see Figure 5). The inclination angle was determined to be constant throughout the machining and was δ = 1.10946°. This angle ensured that the surface machining process was carried out with the greatest efficiency. Consequently, the real cutting speed v_c at the CP_i contact point of the shaping of the machined surface was 71 m/min. In addition, two criteria were used as follows: uniformly distributed roughness $Rth = R_{thvf}$ (i.e., the theoretical roughness has the same value in the feed direction as in the direction perpendicular to it), and a wear limit criterion of VB_{Blim} = 0.2 mm was adopted. The machining parameters for this stage are shown in Table 1.

Table 1. Cutting conditions for the first stage of the research.

Inclination Angle δ [°]	Work Angle of Cutting Blade ψ_{r_rci} [°]	Distance Between Toolpaths b_r [mm]	Axial Depth of Cut a_p [mm]	Feed per Tooth f_z [mm/z]	Cutting Speed (at p. CP_i) v_c [m/min]	Criterion $Rth = R_{thvf}$ [mm]	Criterion VB_{Blim} [mm]
1.10946	23.4411	1.6	0.3	0.1549	71	0.0015	0.2

In order to obtain more accurate test results, the second stage of the model tests, i.e., wear calibration, was carried out. A relationship was established between the maximum allowable cutting time (MACT) at the CP_i contact point of the cutter and its axial distance from the *TCP* vertex. The relationship was established with constant machining parameters (spindle speed and feed rate) in relation to a fixed tool wear threshold, VB_{Blim} = 0.2 mm. For the calibration test, the method described by Altintas [40] was adopted, and Figure 7 shows a simple test setup; by continuously machining at a constant angle δ until tool wear reached a threshold of 0.2 mm, MACT was obtained for a cutter axis orientation of 1.10946°. The machining parameters for the calibration test are shown in Table 2. Each of the machinability and calibration tests was repeated three times, after which the average was calculated. On the basis of the data thus obtained, a tool life model was determined.

Table 2. Cutting conditions for tool wear calibration.

Test No.	Cutting Speed (at p. CP_i) v_c [m/min]	Feed Rate f [mm/rev]	Measured Tool Life T_c [min]
1	40	0.4	84
2	140	0.4	0.97
3	140	0.2	3.7

Tool wear values are similar for the same milling parameters. In each iteration, measurements were carried out at the same fixed points on the time axis. At these points, the differences in wear values did not exceed 10%.

3.3. Measuring and Auxiliary Equipment

In the conception of the proposed solution, in addition to the development of wear and tool life models, it is also necessary to establish a measurement reference on the circular cutting insert and, relative to it, to make the necessary measurements of the angular position using the cutting blade work angle parameter. In addition, the measurement systems and strategies used should allow for the assessment of blade wear.

The xTool F1 laser system on the equipment of the Department of Industrial Engineering and Informatics seated in Prešov was used to determine the measurement reference on the round cutting insert, as shown in Figure 9.

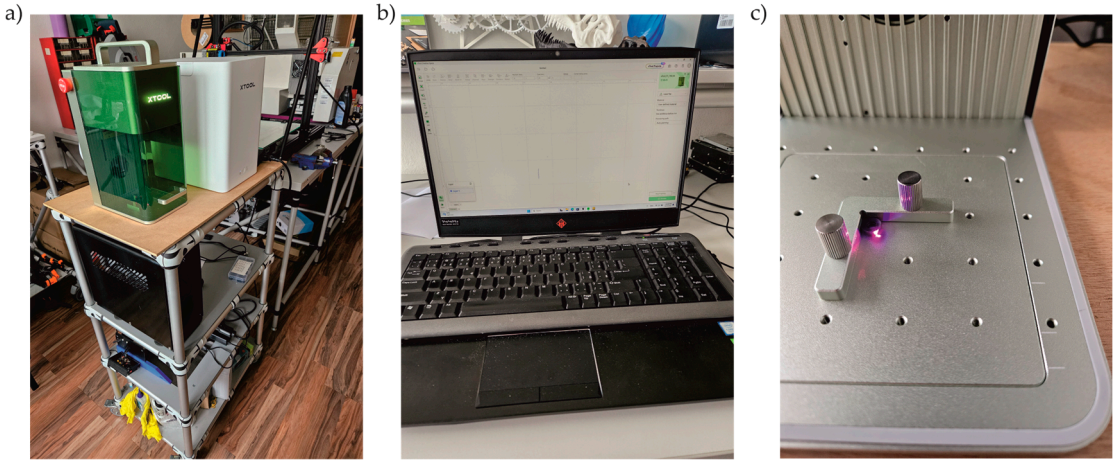

Figure 9. Laser engraving workstation: (**a**) xTool F1 machine; (**b**) PC workstation with xTool Creative Space software (v2.2.23); (**c**) working space with fixed round cutting insert visible laser dot.

It is a system that ensures the engraving of any curve by the action of a laser beam on any part geometry made of any material. The beam movement is programmed in the planar

module of the dedicated xTool Creative Space software. The most important parameters of the reference line application are shown in Table 3.

Table 3. Laser setting parameters.

Laser Set	Movement Accuracy [mm]	Repeat Positioning Accuracy [mm]	Up to Working Speed [mm/s]
2 W 1064 nm	0.00199	0.000248	84

The xTool F1 laser was used to apply an engraving of a line passing through the center of the round cutting insert. A coordinate system was established in the center of the insert based on automatically determined edge outlines. The line itself in the subsequent measurement steps on the microscope served as a reference for measuring the working angle of the blade and the angular positioning in the torus cutter body. The positioning error of the laser spot is 0.000248 mm—therefore negligible in the further stages of testing and positioning.

The proper setting of the round cutting insert in the torus milling cutter body and its subsequent angular positioning after reaching the VB_{Blim} threshold, according to the prepared models, was performed using a KEYENCE VHX 7000 digital microscope (Keyence International, Mechelen, Belgium), which is equipped by the Department of Automobile and Manufacturing Technologies seated in Prešov, as shown in Figure 10. The measurement parameters are shown in Table 4.

Figure 10. Digital 3D microscope used for angular positioning and evaluation of the cutting blade wear.

Table 4. Measurement equipment and parameters.

Microscope	Keyence VHX 7000
Lens	ZS-20 with 20–200× zoom
Shooting mode	4K 3D HDR scanning mode with glare reduction
Magnification	merging images at 100× zoom
Room temperature	22 °C
Humidity	55%

The wear measurements of VB_B along a segment of the active cutting edge were started by determining the outline of this edge. First, the plane tangent to the uppermost

outline of the round cutting insert was determined. From this, the center point that lies in the axis of the insert hole was determined. The error in the displacement of the reference line traced by the laser beam relative to the designated point was then checked. This error did not exceed 0.02 mm. This value did not exceed the minimum threshold of the measure values for tool wear and the work angle of the cutting blade.

4. Results and Discussion

4.1. Procedure for Angular Positioning of the RCI of the Torus Milling Cutter

In order to be able to carry out angular positioning of the RCI of the torus milling cutter, a procedure for the proposed solution was developed, as shown in Figure 11. This procedure takes into account the basic restriction of tool wear and is dedicated to the multi-axis milling process.

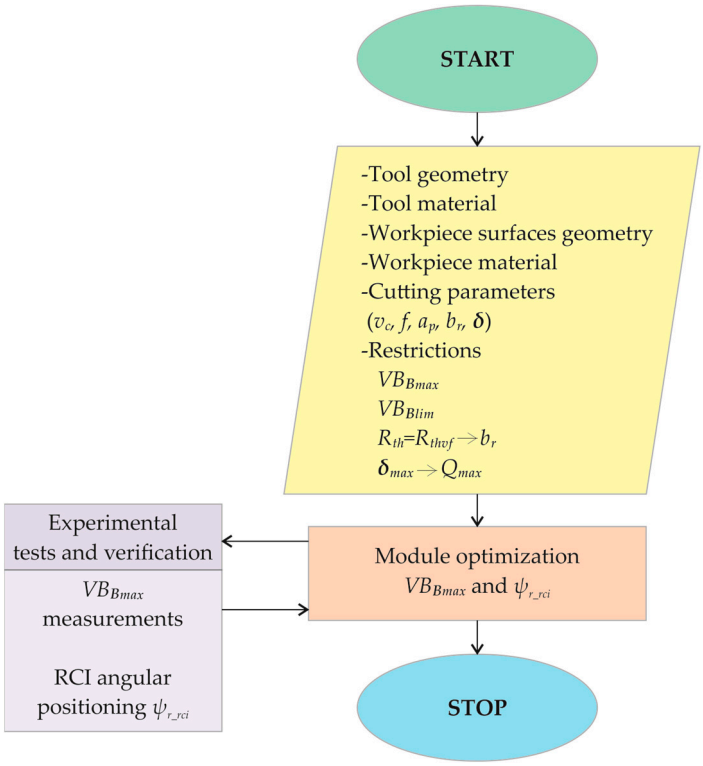

Figure 11. General procedure for the angular positioning of the RCI.

In terms of multi-axis machining, this procedure aims to maximize the volumetric efficiency of the cutting process while fully exploiting the cutting capacity of the tool over its lifetime, as described by the wear parameter. This makes it possible, on the one hand, to use cutting parameters in the HSM range and, on the other, to use the cutting edge length on the periphery of the insert in a controlled and complete manner. This makes the overall tool life significantly longer.

4.2. Tool Wear and Tool Life Models

The development of a concept for an angular positioning method for the round cutting insert of a torus milling cutter begins the wear modeling stage. When modeling tool wear, all three phases of the wear curve were taken into account. This is evident from the resulting classic three-phase wear curve that was obtained for the adopted machining conditions, as shown in Figure 12a. To clarify, it should be mentioned that this drawing shows the first of the three machining tests carried out. The higher number of tests performed is due to the generally accepted principles of statistical analysis and to increase the accuracy of the final model.

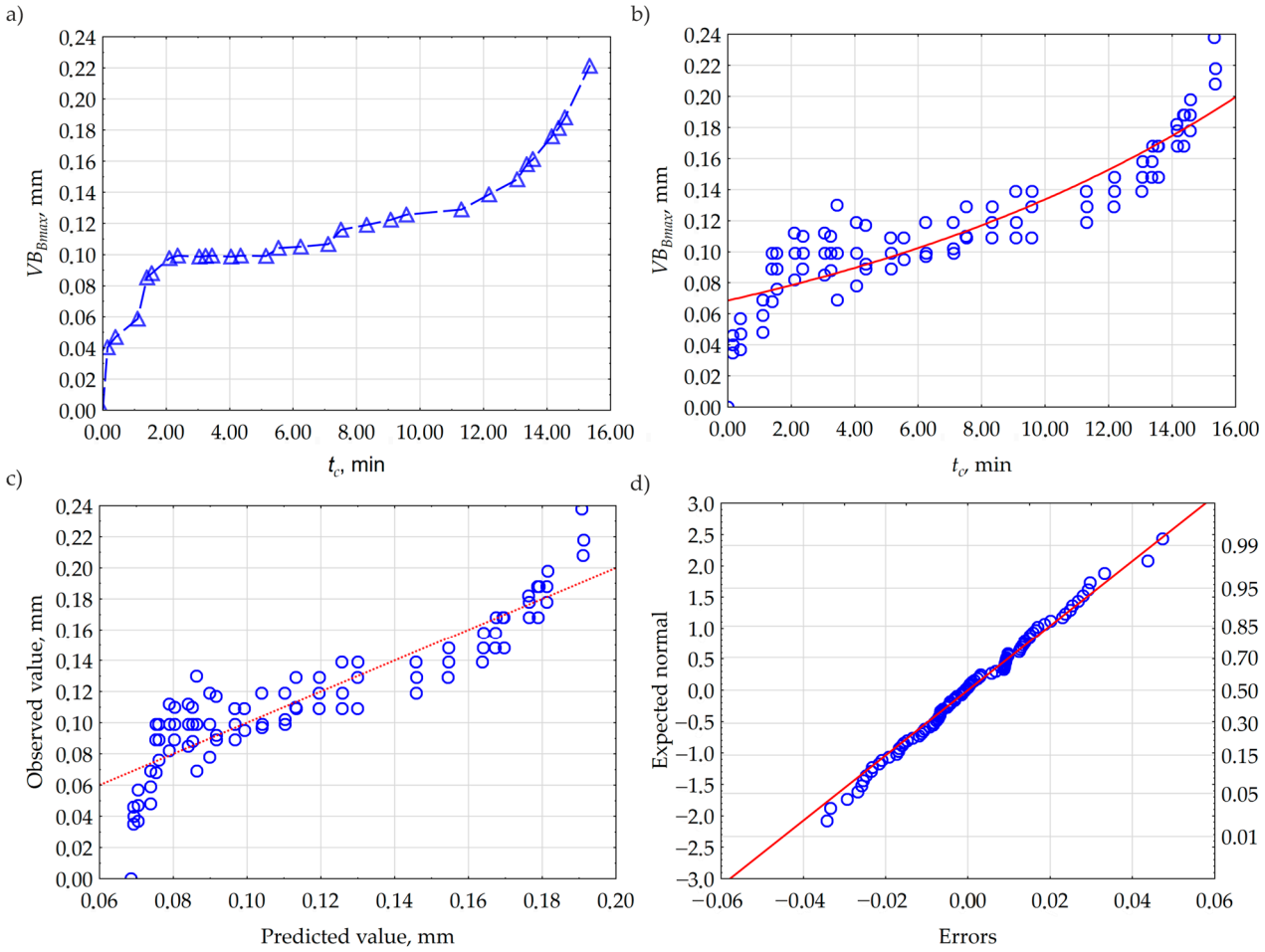

Figure 12. Results of non-linear estimation: (**a**) wear curve; (**b**) fitted model function and observed values; (**c**) scatter plot; (**d**) error normality chart.

As mentioned, wear modeling was carried out using an advanced non-linear ANOVA estimation, as the data obtained cannot be transformed into a linear model. Non-linear estimation involves calculating the relationship between a set of independent variables (i.e., cutting time t_c) and the dependent variable (i.e., tool wear VB_{Bmax}). It was assumed that the wear was evenly distributed over the individual cutting blades, i.e., only one cutting blade is active in the individual feed motion sequences, as also observed by Kita [41].

Analyzing the resulting data set, it was found that it could be approximated by an exponential function model, as described by Equation (10). This is an assumed estimated function. The Least-Squares Method (LSM) was adopted as the loss function, while the Levenberg–Marquardt algorithm was used as the estimation method. The method solves a system of linear equations in each iteration to calculate the gradient. A maximum number of iterations of 6000 was adopted, with a convergence criterion of six decimal places. Based on the above, a model relationship was obtained, which is described by Equation (15).

$$VB_{Bmax} = 0.0685797 \cdot 1.06903^{t_c}, \quad (15)$$

Table 5 shows the estimation statistics and results of the ANOVA analysis of variance.

Table 5. Estimation statistics and results of ANOVA analysis of variance.

	Sum of Squares	Degrees of Freedom	Mean Square	*F*-Value	*p*-Value	*R*
Regression	1.3271	2.0	0.6635	1867.4383	0.0000	0.90
Residual	0.0305	86	0.0003			
Total	1.3577	88				
Adjusted grand total	0.1675	87				
Regression of the adjusted total	1.3271	2.0	0.6635	344.5687	0.0000	

However, Figure 12b–d show the fitted model function and the observed values, a scatter plot of the observed values against the predicted values, and a probability normality plot, respectively.

Based on the results obtained and the analysis of variance, it was concluded that, within the assumed range of variables under study, the developed model is adequate (F = 344.5687) and approximates the predictor variable, i.e., tool wear during cutting, with an accuracy of 90%. This is evidenced by a determination coefficient of R = 0.90. Furthermore, in the scatter plot (Figure 12c), the points lay along a straight line, indicating that the model is appropriate and that the residuals (i.e., errors) are subject to a normal distribution, which, in turn, is illustrated in Figure 12d.

Subsequently, a tool life model was developed for HSM machining, that is, in the range adopted in this work according to Table 2. As a result of the machining tests, the so-called calibration, and after performing the necessary calculations, the tool life is described by Equation (16).

$$T_{c,0.00075} = 4.2 \cdot 10^{6,2} \left(\frac{2\pi n \left(R_T + \sqrt{2 r_p g - g^2} \right)}{1000} \right)^{3.561149} f^{1.931468}, \quad (16)$$

Again, an adequate model was obtained, since for an assumed threshold of VB_{Blim} = 0.2 mm, the lifetime T_c for the CP_i point (g = 0.00075 mm) is 16.353177 min.

4.3. Measurements and APofRCI

The next stage in the development of the concept for the angular positioning method of a circular cutting insert (APofRCI) torus cutter was the measurements.

In order to be able to carry out an angle measurement, i.e., measure the angle of the blade in the base plane under given machining conditions, a reference line must first be marked. This line is applied to a round cutting insert. It passes through the center point of the RCI. In this way, when assembling the tool set (body with inserts), it is possible to position the insert for the first time in such a way that the reference line is parallel from the tool's axis of rotation, as shown in Figure 13. As can be observed in Figure 13b, the marked trace of the cross-sectional effect of the cut layer on the cutting blade is completely within the limits of the cutting blade working angle.

Subsequently, each successive angular positioning of the RCI was realized according to the model dependencies once the limit value VB_{Blim} was reached. Machining tests, together with angular positioning, were repeated two more times, obtaining three active segments worn on the cutting edge, as illustrated in Figure 14.

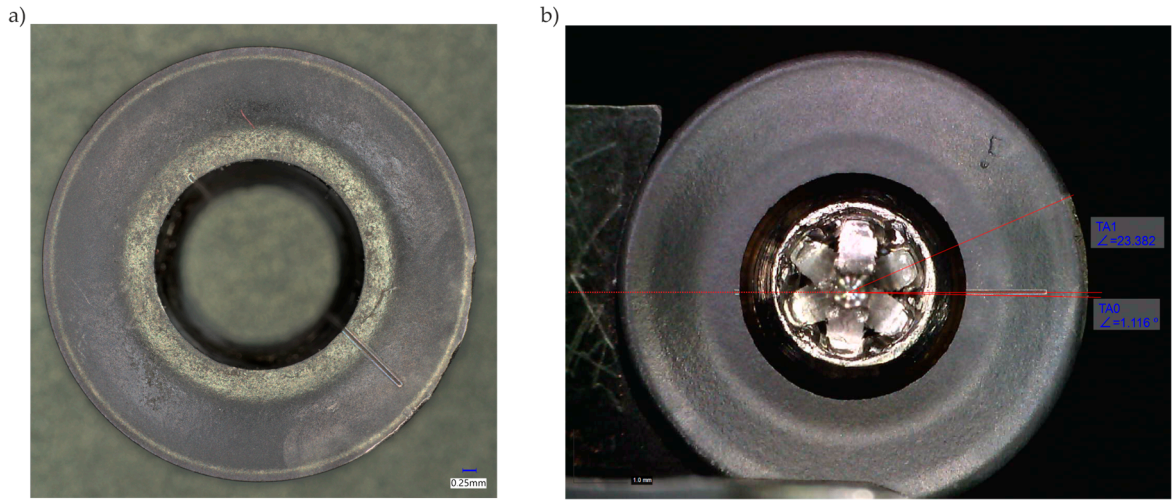

Figure 13. Round cutting insert: (**a**) after laser marking; (**b**) assembled in the cutter body and subjected to a first measurement verification after the first 20 s of operation.

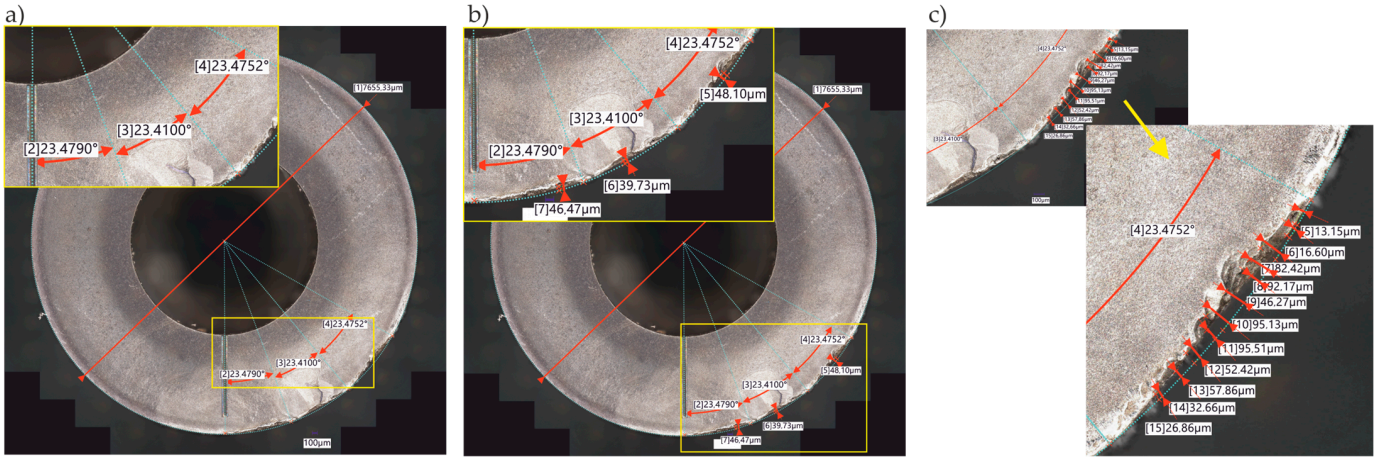

Figure 14. Measurement results: (**a**) correctness of angular positioning; (**b**) maximum defect values for the segments obtained; (**c**) distribution of defect values along the worn active cutting edge.

Analyzing the results obtained from the digital microscope measurement, it was found that all worn segments were within the cutting blade working angle (Figure 14a). This demonstrates the correctness of both the models developed and the procedure together with the measurement techniques used. These techniques made it possible to measure the maximum defect, that is, the abrasion of the blade material, as shown in Figure 14b. It was found that there were differences in the value of the maximum abrasion between the segments, which may be due to the radial runout of the cutting blade. In this case, further research and clarification of the proposed solution should be carried out. In addition, it was also possible to measure the distribution of clash variation relative to the nominal RCI outline, which, in turn, is shown in Figure 14c. Maximum abrasion values were obtained in the zone of maximum thickness of the cut layer acting on the cutting blade. And, in this case, further research is needed. In conclusion, it can be said that the proposed solution works well not only for angular positioning of the RCI but also for carrying out analysis on wear mechanisms.

5. Conclusions

This paper proposes a method for angular positioning of a round cutting insert in a torus cutter body. The method is dedicated to the process of multi-axis milling of sculptured surfaces, but it can also be successfully adopted for other variants of milling as well as

turning using the round cutting insert. The topic addressed in this paper is new and, according to the current state of knowledge, is being tackled for the first time.

The novelty of this work, in addition to the method of angular positioning of the round cutting insert, is above all the comprehensive approach in terms of machinability and tool wear, so that the presented procedure can be used for any workpiece–tool materials pair. In addition, the proposed solution allows the full cutting capability of the entire edge length of the round cutting insert to be fully and predictably over time. The solution is essentially based on the tool wear model developed as part of this work, the tool life model, the way round cutting inserts are labeled and assembled, and the wear measurement methodology.

Taking the above into account, a procedure was developed for the angular positioning of the round cutting insert in a torus cutter body. Based on the results obtained and the analyses carried out, the following key conclusions were drawn:

- The adopted function for approximating tool wear over its lifetime is adequate and provides 90% prediction accuracy;
- The tool life model developed is essentially based on the cutting blade working angle parameter. This makes it possible to predict tool life for different machining conditions and for individual instantaneous positions of the cutting edge in relation to the workpiece surface (3D analysis), which is the subject of further work;
- The developed procedure for angular positioning and measurement enables the entire cutting edge of the blade to be fully utilized, so that the total lifespan of the tool as an assembly is significantly extended;
- The proposed solution also allows measurement and analysis of wear mechanisms, which significantly extends the possibilities of angular positioning of the RCI, taking into account its macro- and micro-geometric characteristics.
- The method proposed in this paper was developed for a specific pair of materials, while the method procedure can be successfully applied to any other pair of workpiece–tool material pair.

The results obtained allowed us to direct further research in the area of tool wear and, more specifically, the prediction of 'notching' wear, which in this work was identified as the highest value of the defect between the worn edge and the nominal outline of the RCI from the measurements.

The research leading to these results was carried out within the framework of international cooperation and Michał Gdula's research internship abroad.

Author Contributions: Conceptualization. M.G. and J.H.; methodology. M.G.; measurements. M.G. and R.V.; modeling and validation. M.G.; formal analysis. M.G.; investigation. M.G., J.H. and R.V.; resources. M.G., L.K. and J.H.; data curation. M.G. and J.H.; writing—original draft preparation. M.G.; writing—review and editing. L.K. and J.H.; visualization. M.G.; supervision. L.K.; project administration. M.G.; funding acquisition. M.G. and L.K. All authors have read and agreed to the published version of the manuscript.

Funding: This research received no external funding.

Institutional Review Board Statement: Not applicable.

Informed Consent Statement: Not applicable.

Data Availability Statement: The original contributions presented in the study are included in the article, further inquiries can be directed to the corresponding author.

Conflicts of Interest: The authors declare no conflicts of interest.

References

1. Escudero, G.G.; Bo, P.; González-Barrio, H.; Calleja-Ochoa, A.; Bartoň, M.; De Lacalle, L.N.L. 5-Axis Double-Flank CNC Machining of Spiral Bevel Gears via Custom-Shaped Tools—Part II: Physical Validations and Experiments. *Int. J. Adv. Manuf. Technol.* **2022**, *119*, 1647–1658. [CrossRef]
2. Bo, P.; González, H.; Calleja, A.; De Lacalle, L.N.L.; Bartoň, M. 5-Axis Double-Flank CNC Machining of Spiral Bevel Gears via Custom-Shaped Milling Tools—Part I: Modeling and Simulation. *Precis. Eng.* **2020**, *62*, 204–212. [CrossRef]
3. González, H.; Calleja, A.; Pereira, O.; Ortega, N.; Norberto López de Lacalle, L.; Barton, M. Super Abrasive Machining of Integral Rotary Components Using Grinding Flank Tools. *Metals* **2018**, *8*, 24. [CrossRef]
4. González, H.; Pereira, O.; Fernández-Valdivielso, A.; López De Lacalle, L.; Calleja, A. Comparison of Flank Super Abrasive Machining vs. Flank Milling on Inconel® 718 Surfaces. *Materials* **2018**, *11*, 1638. [CrossRef]
5. Sliusarenko, O.; Escudero, G.G.; González, H.; Calleja, A.; Bartoň, M.; Ortega, N.; De Lacalle, L.N.L. Constant Probe Orientation for Fast Contact-Based Inspection of 3D Free-Form Surfaces Using (3+2)-Axis Inspection Machines. *Precis. Eng.* **2023**, *84*, 37–44. [CrossRef]
6. Wang, J.; Luo, M.; Xu, K.; Tang, K. Generation of Tool-Life-Prolonging and Chatter-Free Efficient Toolpath for Five-Axis Milling of Freeform Surfaces. *J. Manuf. Sci. Eng.* **2019**, *141*, 031001. [CrossRef]
7. Zeng, H.; Yan, R.; Du, P.; Zhang, M.; Peng, F. Notch Wear Prediction Model in High Speed Milling of AerMet100 Steel with Bull-Nose Tool Considering the Influence of Stress Concentration. *Wear* **2018**, *408–409*, 228–237. [CrossRef]
8. An, Q.; Cai, C.; Zou, F.; Liang, X.; Chen, M. Tool Wear and Machined Surface Characteristics in Side Milling Ti6Al4V under Dry and Supercritical CO_2 with MQL Conditions. *Tribol. Int.* **2020**, *151*, 106511. [CrossRef]
9. Ni, C.; Wang, X.; Zhu, L.; Liu, D.; Wang, Y.; Zheng, Z.; Zhang, P. Machining Performance and Wear Mechanism of PVD TiAlN/AlCrN Coated Carbide Tool in Precision Machining of Selective Laser Melted Ti6Al4V Alloys under Dry and MQL Conditions. *J. Manuf. Process.* **2022**, *79*, 975–989. [CrossRef]
10. Gdula, M.; Mrówka-Nowotnik, G. Analysis of Tool Wear, Chip and Machined Surface Morphology in Multi-Axis Milling Process of Ni-Based Superalloy Using the Torus Milling Cutter. *Wear* **2023**, *520–521*, 204652. [CrossRef]
11. Luo, M.; Luo, H.; Zhang, D.; Tang, K. Improving Tool Life in Multi-Axis Milling of Ni-Based Superalloy with Ball-End Cutter Based on the Active Cutting Edge Shift Strategy. *J. Mater. Process. Technol.* **2018**, *252*, 105–115. [CrossRef]
12. Cao, L.-X.; Gong, H.; Liu, J. The Offset Approach of Machining Free Form Surface. *J. Mater. Process. Technol.* **2007**, *184*, 6–11. [CrossRef]
13. Musfirah, A.H.; Ghani, J.A.; Haron, C.H.C. Tool Wear and Surface Integrity of Inconel 718 in Dry and Cryogenic Coolant at High Cutting Speed. *Wear* **2017**, *376–377*, 125–133. [CrossRef]
14. Zhu, Z.; Peng, F.; Yan, R.; Li, Z.; Wu, J.; Tang, X.; Chen, C. Influence Mechanism of Machining Angles on Force Induced Error and Their Selection in Five Axis Bullnose End Milling. *Chin. J. Aeronaut.* **2020**, *33*, 3447–3459. [CrossRef]
15. Chang, Z.; Qian, J.; Chen, Z.C.; Wan, N.; Zhang, D. Geometrical Theory of Cutting Stock with Torus End Mills in Five-Axis CNC Machining and Its Applications in Machining Simulation. *Int. J. Adv. Manuf. Technol.* **2019**, *105*, 27–46. [CrossRef]
16. Gao, W.; Kim, S.W.; Bosse, H.; Haitjema, H.; Chen, Y.L.; Lu, X.D.; Knapp, W.; Weckenmann, A.; Estler, W.T.; Kunzmann, H. Measurement Technologies for Precision Positioning. *CIRP Ann.* **2015**, *64*, 773–796. [CrossRef]
17. Ivanov, V.; Botko, F.; Dehtiarov, I.; Kočiško, M.; Evtuhov, A.; Pavlenko, I.; Trojanowska, J. Development of Flexible Fixtures with Incomplete Locating: Connecting Rods Machining Case Study. *Machines* **2022**, *10*, 493. [CrossRef]
18. Brillinger, M.; Wuwer, M.; Abdul Hadi, M.; Haas, F. Energy Prediction for CNC Machining with Machine Learning. *CIRP J. Manuf. Sci. Technol.* **2021**, *35*, 715–723. [CrossRef]
19. Ramos-Fernández, J.C.; López-Morales, V.; Márquez-Vera, M.A.; Pérez, J.M.X.; Suarez-Cansino, J. Neuro-Fuzzy Modelling and Stable PD Controller for Angular Position in Steering Systems. *Int. J. Automot. Technol.* **2021**, *22*, 1495–1503. [CrossRef]
20. Kaščak, J.; Gašpár, Š.; Paško, J.; Husár, J.; Knapčíková, L. Polylactic Acid and Its Cellulose Based Composite as a Significant Tool for the Production of Optimized Models Modified for Additive Manufacturing. *Sustainability* **2021**, *13*, 1256. [CrossRef]
21. Abdul Hadi, M.; Brillinger, M.; Wuwer, M.; Schmid, J.; Trabesinger, S.; Jäger, M.; Haas, F. Sustainable Peak Power Smoothing and Energy-Efficient Machining Process Thorough Analysis of High-Frequency Data. *J. Clean. Prod.* **2021**, *318*, 128548. [CrossRef]
22. Abdul Hadi, M.; Kraus, D.; Kajmakovic, A.; Suschnigg, J.; Guiza, O.; Gashi, M.; Sopidis, G.; Vukovic, M.; Milenkovic, K.; Haslgruebler, M.; et al. Towards Flexible and Cognitive Production—Addressing the Production Challenges. *Appl. Sci.* **2022**, *12*, 8696. [CrossRef]
23. Visan, D.A.; Lita, I.; Cioc, I.B. Wireless Control System for Angular Positioning Applications. In Proceedings of the 2013 IEEE 19th International Symposium for Design and Technology in Electronic Packaging (SIITME), Galati, Romania, 24–27 October 2013; pp. 103–106.
24. Adamczak, M.; Kolinski, A.; Trojanowska, J.; Husár, J. Digitalization Trend and Its Influence on the Development of the Operational Process in Production Companies. *Appl. Sci.* **2023**, *13*, 1393. [CrossRef]
25. Hrehova, S. Description of Using Different Software Tools to Analyze the Selected Process. In Proceedings of the 2019 20th International Carpathian Control Conference (ICCC), Krakow-Wieliczka, Poland, 26–29 May 2019; pp. 1–5.
26. Coranic, T.; Mascenik, J. Experimental Measurement of Dynamic Characteristics of Structural Units. *Processes* **2023**, *11*, 3333. [CrossRef]

27. Jurko, J.; Miškiv-Pavlík, M.; Hladký, V.; Lazorík, P.; Michalík, P.; Petruška, I. Measurement of the Machined Surface Diameter by a Laser Triangulation Sensor and Optimalization of Turning Conditions Based on the Diameter Deviation and Tool Wear by GRA and ANOVA. *Appl. Sci.* **2022**, *12*, 5266. [CrossRef]
28. Jurko, J.; Miškiv-Pavlík, M.; Husár, J.; Michalik, P. Turned Surface Monitoring Using a Confocal Sensor and the Tool Wear Process Optimization. *Processes* **2022**, *10*, 2599. [CrossRef]
29. Tran, C.-S.; Hsieh, T.-H.; Jywe, W.-Y. Laser R-Test for Angular Positioning Calibration and Compensation of the Five-Axis Machine Tools. *Appl. Sci.* **2021**, *11*, 9507. [CrossRef]
30. Yi-Tsung, L.; Kuang-Chao, F. A Novel Method of Angular Positioning Error Analysis of Rotary Stages Based on the Abbe Principle. *Proc. Inst. Mech. Eng. Part B J. Eng. Manuf.* **2018**, *232*, 1885–1892. [CrossRef]
31. Kanno, Y.; Sato, Y. Linear and Angular Position Sensing for Two- Degrees-of-Freedom Motor. *Int. J. Smart Sens. Intell. Syst.* **2014**, *7*, 1–6. [CrossRef]
32. Chen, H.; Jiang, B.; Lin, H.; Zhang, S.; Shi, Z.; Song, H.; Sun, Y. Calibration Method for Angular Positioning Deviation of a High-Precision Rotary Table Based on the Laser Tracer Multi-Station Measurement System. *Appl. Sci.* **2019**, *9*, 3417. [CrossRef]
33. Gietler, H.; Stetco, C.; Zangl, H. Scalable Retrofit Angular Position Sensor System. In Proceedings of the 2020 IEEE International Instrumentation and Measurement Technology Conference (I2MTC), Dubrovnik, Croatia, 25–28 May 2020; pp. 1–6.
34. Sridharan, M.; Dhandapani, S. Real Time Embedded System Development for Missile Angular Position Acquisition through Image Processing. *CSIT* **2020**, *8*, 257–261. [CrossRef]
35. Diakov, D.; Komarski, D. Micro-Positioning Module for Angular Orientation Position of the Axis of Rotation Analysis. In Proceedings of the 2021 XXXI International Scientific Symposium Metrology and Metrology Assurance (MMA), Sozopol, Bulgaria, 7–11 September 2021; pp. 1–6.
36. Marciniak, K. Influence of Surface Shape on Admissible Tool Positions in 5-Axis Face Milling. *Comput. Aided Des.* **1987**, *19*, 233–236. [CrossRef]
37. Lazoglu, I.; Liang, S.Y. Modeling of Ball-End Milling Forces With Cutter Axis Inclination. *J. Manuf. Sci. Eng.* **2000**, *122*, 3–11. [CrossRef]
38. Knapčíková, L.; Dupláková, D.; Radchenko, S.; Hatala, M. Rheological Behavior Modelling of Composite Materials Used in Engineering Industry. *TEM J.* **2017**, *6*, 242–245. [CrossRef]
39. Pavlenko, I.; Piteľ, J.; Ivanov, V.; Berladir, K.; Mižáková, J.; Kolos, V.; Trojanowska, J. Using Regression Analysis for Automated Material Selection in Smart Manufacturing. *Mathematics* **2022**, *10*, 1888. [CrossRef]
40. Altintas, Y. *Manufacturing Automation. Metal Cutting Mechanics, Machine Tool Vibrations, and CNC Design*, 2nd ed.; Cambridge University Press: New York, NY, USA, 2012; ISBN 978-0-521-17247-9.
41. Kita, Y.; Furuike, H.; Kakino, Y.; Nakagawa, H.; Hirogaki, T. Basic Study of Ball End Milling on Hardened Steel. *J. Mater. Process. Technol.* **2001**, *111*, 240–243. [CrossRef]